November 10, 1998

Physics Design of the National Spherical Torus Experiment

S.M. Kaye[1], M. Ono[1], Y.-K.M. Peng[2], D.B. Batchelor[2], M.D. Carter[2], W. Choe[3], R. Goldston[1], Y.S. Hwang[3], E.F. Jaeger[2], T. Jarboe[4], S. Jardin[1], D. Johnson[1], R. Kaita[1], C. Kessel[1], H. Kugel[1], R. Maingi[2], R. Majeski[1], J. Manickam[1], J. Menard[1], D.R. Mikkelsen[1], D. Orvis[4], B. Nelson[4], F. Paoletti[5], N. Pomphrey[1], G. Rewoldt[1], S. Sabbagh[5], D.J. Strickler[2], E. Synakowski[1], J.R. Wilson[1]

Abstract

The mission of the National Spherical Torus Experiment (NSTX) is to prove the principles of spherical torus physics by producing high-β_t plasmas that are non-inductively sustained, and whose current profiles are in steady-state. NSTX will be one of the first ultra low aspect ratio tori ($R/a \leq 1.3$) to operate at high power (P_{input} up to 11 MW) in order to produce high-β_t (25 to 40%), low collisionality, high bootstrap fraction ($\leq$70%) discharges. Both RF and NB heating and current drive will be employed. Built into NSTX is sufficient configurational flexibility to study a range of operating space and the resulting dependences of the confinement, micro- and MHD stability, and particle and power handling properties. NSTX research will be carried out by a nationally based science team.

[1]Princeton Plasma Physics Laboratory, Princeton University, Princeton, N.J. 08543
[2]Oak Ridge National Laboratory, Oak Ridge, Tenn. 37830
[3]KAIST, Taejon, Korea
[4]Univ. of Washington, Seattle, Wash. 98105
[5]Dept. of Applied Physics, Columbia Univ., NYC, N.Y. 10027

I. Introduction

Spherical Tori (ST) can potentially provide an attractive path to a reactor or Volumetric Neutron Source (VNS). The ST fusion core would be small, economic, high power density, and with the use of a copper toroidal field coil inner leg and without a large inboard shield and OH transformer, it would be a simple and reliable system. With encouraging experimental results from present low aspect ratio experiments such as START,[1] CDX-U,[2] and HIT,[3] and encouraging theoretical predictions,[4–6] the National Spherical Torus Experiment (NSTX) has been approved and is presently under construction. Various reactor concepts have been advanced for the ST,[7,8] and these have identified issues of importance in the development of ST-based fusion power. NSTX will address many of these issues, including transport and confinement, MHD stability, non-inductive operation and power and particle handling.

The overall goal of NSTX is to prove the principles of ST physics in a 1 MA device that can produce high-β_t plasmas in non-inductively sustained discharges whose current profile is in steady-state, with an aim towards creating a cost-effective pathway to a fusion core. It is the set of issues related to developing an attractive ST fusion core that forms the basis for the performance objectives of NSTX. The purpose of this paper is to present the physics basis for the design of NSTX, along with the hardware capabilities required to achieve of these performance objectives and thus pave the way for continued development of the ST concept. 0-D calculations that elucidate some of the key ST physics/fusion core issues will be presented in the next section, followed by a discussion of the resulting experimental objectives, baseline device capabilities, and the general physics basis for exploring the ST configuration in NSTX. Following this, the details of the physics calculations in the areas of configurational flexibility, confinement and transport, MHD stability and β_t-limits, heating and current drive, and power and particle handling will be presented. Finally, there will be a brief discussion of the planned diagnostics and preliminary Research Plan.

II. 0-D Considerations

Some of the key advantages of the ST configuration, along with some of the issues, can be seen from simple 0-D considerations. We start from the definition of fusion yield,

$$P_{fusion} \simeq Vol \cdot (nT)^2 \cdot \frac{<\sigma v>}{T^2} \simeq Vol \cdot B_0^4 \cdot \beta_t^2 \cdot \frac{<\sigma v>}{T^2} \qquad (1)$$

Here, and throughout the paper, β_t is defined as $2\mu_0 < p > /B_0^2$, B_0 being the vacuum

toroidal magnetic field at the geometric radius. The cost of a fusion core depends on the volume and the magnetic field; the fusion cross-section and plasma temperature are dependent on the plasma properties. One way to reduce the cost of a fusion core for fixed volume is to reduce the magnetic field, B_0, which can be done if β_t is high enough.[6]

It is often convenient to express the stability limit for the plasma β_t as

$$\beta_t = \beta_n \frac{I_p}{a B_0} \tag{2}$$

where $I_p$is plasma current, a is plasma minor radius, and β_n is a constant which is typically two to four in conventional aspect ratio tokamaks. The advanced physics regimes have achieved or are predicted to attain a β_n of four to six. The MHD analyses of low-aspect-ratio tori have led to predicted values of β_n from four to above eight for optimized current and pressure profiles and with the presence of a nearby conducting shell.[4] It is clear from Eq. 2 that raising the plasma current increases β_t for a given β_n. The plasma current increases dramatically at fixed q(a) as the aspect ratio is reduced, as can be seen from the relation

$$I_p \simeq \frac{1+\kappa^2}{2} \frac{R_0 B_0}{q(a)} \frac{A f(A)}{(A^2-1)^2} \tag{3}$$

where κ is the elongation, R_0 is the plasma major radius, q(a) is the inverse rotational transform at the plasma edge, $A = R_0/a$, and $f(A) = 1.22A - 0.68$.[9] The increase in plasma current with decreasing A is mainly due to the field pitch behavior in the inner part of the torus near the center TF post. As A decreases, the magnetic pitch goes down as $(A^2-1)^2$ since the toroidal field increases and the toroidal circumference decreases while the poloidal magnetic field remains relatively unchanged. The inherent high current nature of the ST plasmas has been demonstrated in the experiments on START[10] and CDX-U.[2]

Higher plasma current is also generally favorable for plasma confinement in strongly heated plasmas. As aspect ratio is reduced at fixed q, the resulting increase in plasma current improves confinement in present day empirical scaling expressions.[11–13]

Incorporating Eq. 2 and Eq. 3 into Eq. 1, one obtains

$$P_{fusion} \propto \beta_n^2 \kappa (1+\kappa^2)^2 \frac{R_0^3 B_0^4}{q(a)^2} \frac{A^2 f(A)^2}{(A^2-1)^4} \tag{4}$$

which illustrates the parameters which most strongly influence the amount of fusion power produced. The fusion power can increase significantly as aspect ratio is reduced. It is also a strong function of plasma elongation.[6] It is well known that as

the aspect ratio is reduced, the plasma elongates naturally without external coils.[9,14] This behavior is a consequence of the strong toriodicity of ST plasmas. The natural elongation is also a strong function of the plasma internal inductance, with κ increasing as l_i is reduced.[15] For ST fusion cores, where it can be quite difficult to create elongation by external coils, it is highly desirable to have this natural elongation to enhance the fusion yield.

Another consideration for fusion power yield is the maximum allowable magnetic field. In a toroidal device, the maximum magnetic field, B_{max}, usually occurs at the outer region of the inner leg of the TF coil, $R_c = R_0 - a - \Delta$. Here, Δ is the distance between the coil and the inner plasma edge. If the coil is a superconducting magnet, B_{max} is typically limited to about 13 T. The normal conductor magnetic field can be significantly higher. Since B_{max} is related to B_T by $B_{max}R_c = B_0R_0$, the fusion power can be rewritten as

$$P_{fusion} \propto \beta_n^2 \kappa (1+\kappa^2)^2 \frac{R_0^3 B_{max}^4}{q(a)^2} \left[\frac{A-1-\Delta/a}{A^2-1}\right]^4 \frac{f(A)^2}{A^2} \tag{5}$$

The gap size should be made as small as possible for maximizing fusion yield. Assuming the gap can be ignored, which is essentially the same as assuming there is no OH solenoid, the equation can be reduced to

$$P_{fusion} \propto \beta_n^2 \kappa (1+\kappa^2)^2 \frac{R_0^3 B_{max}^4}{q(a)^2} \frac{f(A)^2}{(A+1)^4 A^2} \tag{6}$$

The fusion yield favors low aspect ratio both with and without a gap, although optimizing the fusion yield depends on consideration of all the parameters in the above equation.

The final important factor for an ST fusion core that will be considered here is the ratio of fusion power to the resistive power used for the TF magnet. Clearly, it is desirable to minimize the recirculating fusion power. The TF coil resistive dissipation is concentrated in the TF center leg for ST devices. The parametric dependence of the coil resistance can be expressed as

$$P_{TF} \propto \kappa J_{TF}^2 R_0^3 \frac{(A-1-\Delta/a)^2}{A^2} \propto \kappa R_0 B_{max}^2 \tag{7}$$

Therefore, the ratio of the fusion power to the power dissipated in the center leg is

$$\frac{P_{fusion}}{P_{TF}} \propto \beta_n^2 (1+\kappa^2)^2 \frac{R_0^2 B_{max}^2}{q(a)^2} \frac{f(A)^2}{(A+1)^4 A^2} \tag{8}$$

As was found with Eq. 6, this ratio favors low A, although optimization of all the parameters is necessary for minimizing the recirculating power.

III. Experimental Objectives

The 0-D considerations presented in the previous section illustrate some of the physics issues that must be addressed, and performance objectives that must be achieved, in order to advance the ST concept. It is clear that the low aspect ratio configuration must operate at high-β_t, high plasma current, high elongation, and with little or no OH solenoid. To this end, the experimental and performance objectives that have been established for NSTX are:

- Achievement of $\beta_n \geq 4,\ \beta_t \sim 25\%$ at low collisionality for first stability regime plasmas ($q_0 \sim 1.0$).
- Achievement of $\beta_n \geq 8,\ \beta_t \sim 40\%$ at low collisionality in advanced physics scenarios ($q_0 \sim 2.5$).
- Demonstration of non-inductive discharge start-up to current levels of 0.5 MA.
- Demonstration of full non-inductive, steady-state current sustainment with high bootstrap fraction (70%).
- Demonstration of adequate power and particle handling capability at high-β_t and long pulse length.

To achieve these objectives, the NSTX device was designed with the capabilities listed in Table 1.

Achieving high-β_t (25 to 40%) at low collisionality requires adequate confinement and auxiliary heating, and NSTX will be one of the first ultra-low aspect ratio tori ($R/a \leq 1.3$) to operate at high power (P_{input} up to 11 MW). Performance estimates from Neutral Beam Injection (NBI) discharges in START[16] indicate good confinement at low aspect ratio. However, the parametric dependence of energy confinement at low aspect ratio is not yet known, and understanding the confinement scaling and transport physics at low aspect ratio with high heating power, low collisionality and high density is one of the major elements of the NSTX mission. Suppression of electrostatic and electromagnetic microinstabilities due to increased orbit-averaged good curvature, as indicated by code calculations,[5] and the role of the high velocity shearing rate, due to the low toroidal magnetic field, will also be a focus of these confinement and transport studies.

Recent START[1] results have demonstrated the ability of STs to produce high-β_t ($\beta_t \simeq 40\%,\ \beta_0 \simeq 100\%$) in the first stability regime ($q_0 \sim 1$). NSTX will investigate high-β_t ($\geq 25\%$) equilibria, specifically addressing the dependence of the ballooning and kink instabilities on variations in aspect ratio, shaping and the presence

R	0.85 m
a	0.68 m
I_p	1 MA
B_T	0.3 T
κ	2.0
R/a	1.27
Start-Up	OH, ECH, C0-Axial Helicity Injection (CHI)
Wall Stabilization	Close-fitting Conducting Plates
Auxiliary Heating and Current Drive	CHI, HHFW (6 MW), NBI (5 MW)
Profile Control	HHFW, CHI, NBI
Maximum Pulse Length	5 sec. (> current relaxation time)
Divertor	Single- and Double-Null, Inner Wall Limited
Profile Diagnostics	

Table 1: Device Capabilities

of conducting plates. The presence of conducting plates are important for attaining high-β_t; results from PBX and PBX-M[17,18] indicate that passive conducting plates in close proximity to a rotating plasma can reduce the growth rates for low-n global MHD modes, thus enhancing the plasma stability and leading to higher-β values. The conducting plates, however, must be able to withstand escaping heat and particle flux without compromising plasma purity.

High-q, q_0 operation at low collisionality and high-β_t lends itself to high bootstrap current regime investigations, while low-q, q_0 operation will focus on studying the maximum β_t limits for stable, disruption-free operation.

For the high performance plasmas, the β and the shaping factor, S, is typical of what would be required for an ST VNS or reactor. Results from DIII-D[19] indicate that $\beta_t \tau_E$ is a strong function of the shaping parameter, $S = I_p q_\psi / a B_T$. The shaping parameter can be written in the form $S = [A/(A-1)^2](1+\kappa^2)/2$, where the elongation, κ, increases strongly as $A \to 1$, a benefit of the naturally high elongation inherent in ST plasmas. For NSTX plasmas, S is expected to be approximately 80, which is over a factor of ten greater than that of present day conventional aspect ratio tokamaks.

Another capability that is built into NSTX to enable it to achieve its objectives is configurational and shape flexibility. Flexible shape control is required to explore a wide range of plasma elongation and triangularity in order to optimize the plasma stability. Furthermore, it will be necessary to adjust the plasma shape and position

in order to maximize the scrape-off layer (SOL) flux tube expansion under the constraints imposed by the fixed position of the conducting plates and by the required X-point position. The ability to control the plasma shape and position is important for assessing the benefits of low aspect ratio in suppressing microinstabilities believed to be responsible for radial heat and particle transport. Finally, configurational flexibility is crucial to producing a range of divertor configurations; specifically, a single-null configuration is required for Co-axial Helicity Injection (CHI).[3]

The current in an ST fusion core, which can be at levels of tens of MA, must be produced and maintained non-inductively since an ST reactor will not likely be able to support an OH capability due to space and power limitations. The development of non-inductive start-up techniques is therefore crucial to the ST development path. NSTX will, during its first phase of operation, employ CHI as the primary non-inductive start-up technique. CHI has been used successfully on HIT to produce a 200 kA plasma,[3] and extrapolation to NSTX based on injector current to plasma current conversion efficiency indicates that producing a 500 kA plasma is possible. Since CHI is a technology that still needs development in ST plasmas, NSTX is designed with the capability to produce and to drive current inductively in order to ensure that other critical physics can be studied. Approximately 0.9 V-sec are available from the OH windings and Poloidal Field (PF) coil set, with about 2/3 of the total V-sec being produced by the OH. Inductive breakdown will be aided by 20 kW of EC pre-ionization. EC pre-ionization may also be employed to aid CHI startup.

During the main phase of NSTX discharges, 6 MW of High Harmonic Fast Waves (HHFW), and 5 MW of Neutral Beam Injection (NBI) will be the primary auxiliary heating and, along with bootstrap current, the primary non-inductive current drive techniques. At low ion β, the HHFW will preferentially heat electrons.[20] This serves two purposes; the first is to drive current directly, and the second is to increase the bootstrap current fraction that is driven through the hotter electrons. HHFW will provide current profile control through $n_{\|}$ control during the flattop phase of the discharge, although at higher-β_t, the HHFW current will be driven off-axis. Alternatively, NBI driven current will be peaked on axis for the expected plasma densities and beam orientation.

The possibility of driving current during the current sustainment phase in the very outer portion of the plasma with CHI will be explored. As will be seen in a later section, some edge current drive ($\sim$ 25%) is required for producing the necessary profiles for the highest-β_t target.

These different current drive and heating techniques provide the capability for current and pressure profile control, and thus the ability to explore a wide range of operational scenarios in order to both study fundamental ST physics as well as produce high performance ST plasmas.

It is important that the evaluation of the confinement and MHD properties of ST discharges be in a steady-state regime, where the current profiles have had adequate time to fully relax, in order to assess the reactor potential for stable, high-β_t scenarios. Typical 1 MA current flattop durations for inductive operation of NSTX with auxiliary heating range from 150 msec to 0.5 sec., generally depending on the type of heating employed (ion heating with NBI or electron heating with HHFW). A 0.5 MA CHI target plasma would greatly increase the current flattop duration due to savings in inductive V-sec. While the inductive operation pulse lengths may be five to ten times the plasma energy confinement time, the 0.5 sec. current flattop duration is not long enough for the current profile to attain steady-state. Estimates based on the results of a current relaxation study[21] indicate that the time constant for the current profile to relax for typical NSTX parameters is from 1 to 2 sec. for the constant current and voltage boundary conditions, conditions which would be expected during the current sustainment phase of the discharge. Consequently, because the required current relaxation time constant is longer than the inductive current flattop duration, non-inductive current drive is an essential ingredient also in attaining a current profile in steady-state. Furthermore, NSTX was designed for pulse lengths up to 5 sec. for this non-inductive operation, the pulse length limited to this duration by the heating of the center stack TF coil.

Divertor heat loads in STs are expected to be high because of the compact nature of this configuration. The divertor and limiter surfaces in NSTX must be able to handle the power densities produced in the high-β_t, long-pulse discharges with the initial 6 MW of RF heating along with a heating system upgrade to 11 MW (with NBI). Estimates indicate that the baseline 6 MW of heating may result in power densities on the divertor plate of order 15 MW/m^2. The vacuum vessel volume must be adequate to allow plasma configurations that maximize the range of SOL flux tube expansion, which is estimated to be up to a factor of 4. Inertial cooling of the divertor plates, as well as the plasma facing components on other limiting surfaces, is generally adequate for 5 sec. pulse lengths, although at the highest power densities either the pulse lengths will have to be shorter than 5 sec. and/or divertor sweeping will be employed. The machine design can accommodate a divertor cryopump as an upgrade possibility.

Finally, much emphasis will be placed on detailed diagnosis of the plasma characteristics, with specific aims of determining and understanding the MHD stability (including disruption mechanisms), transport and microinstabilities, and divertor characteristics.

In the remainder of this paper, we will present the details of the physics calculations in the areas mentioned above, and this will be followed by a brief discussion of the planned diagnostics and preliminary Research Plan.

IV. Reference Geometry

A cross-section of NSTX is shown in Fig. 1. Some of the notable features to point out include the close-fitting conducting plates, whose purpose is to slow down or stabilize the plasma vertical motion and growth of low-n instabilities, the divertor region, including a slot between the upper conducting plate and outer divertor plate for possible future cryo-pumping, the set of Poloidal Field (PF) coils, and ceramic breaks for isolating vessel segments for CHI. The set of PF coils include five up-down symmetric pairs (PF1a, PF2-5) and one coil, PF1b, which is only in the lower half-plane. PF1b will be used specifically for controlling the X-point and separatrix leg positions in single-null discharges for CHI. It is important, for the success of CHI, to have one separatrix leg on each of the CHI electrodes; each divertor plate on either side of the ceramic break and the PF1b coil constitutes an electrode.

PF3 and PF5 will provide the vertical field necessary for radial control of the plasma, while PF1a, PF2, and also PF3 will be used for controlling the plasma shape. During the initial operation of the device, PF4 will not be used; this coil will be used at a later date to enhance the shape control capability of the device. Table 2 lists the number of turns in the OH and in each PF coil (in each half-plane), and the coil current/turn limit (absolute value) for each. The power supplies associated with each PF coil do not limit the achievable coil current. It is also noted that a more than sufficient number of power supplies exist so that each coil can be controlled separately (i.e., upper and lower), and can have bipolar capability if necessary.

In order to study the uncharted region of ST physics, a great deal of configurational flexibility has been built into NSTX. This flexibility, which includes different plasma shapes at fixed aspect ratio as well as different aspect ratio configurations, will allow exploration of transport characteristics and MHD stability boundaries, and it will also allow for some optimization of the power handling capability and RF coupling. The coil currents necessary for producing the different plasma configurations at fixed aspect ratio are not restricted by coil or power supply limitations. As an

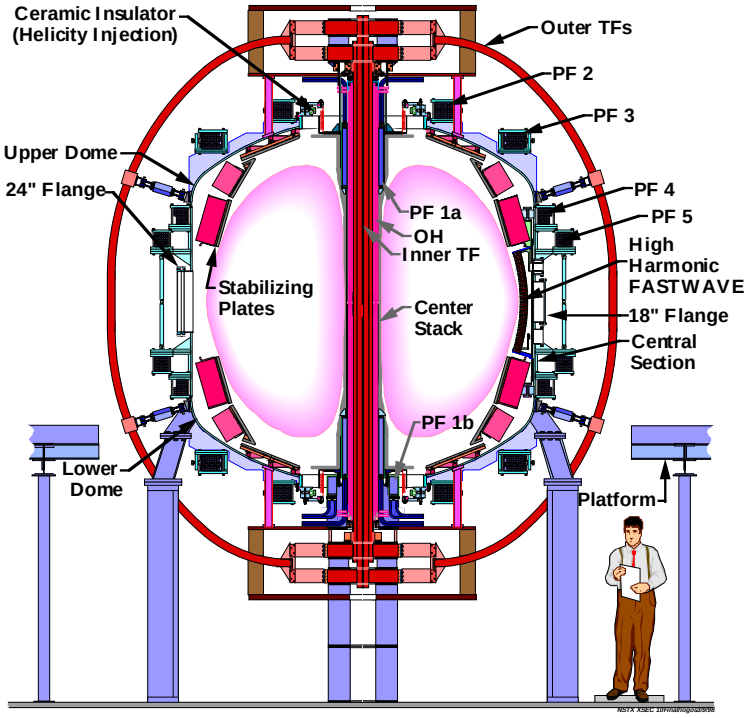

Figure 1: NSTX Cross-Section

Coil	No. Turns	Coil Current/Turn Limit (kA)
OH	482	24
PF1a	48	15
PF1b	36	20
PF2	28	20
PF3	30	20
PF4	22	20
PF5	24	20

Table 2: OH and PF Coil Capabilities

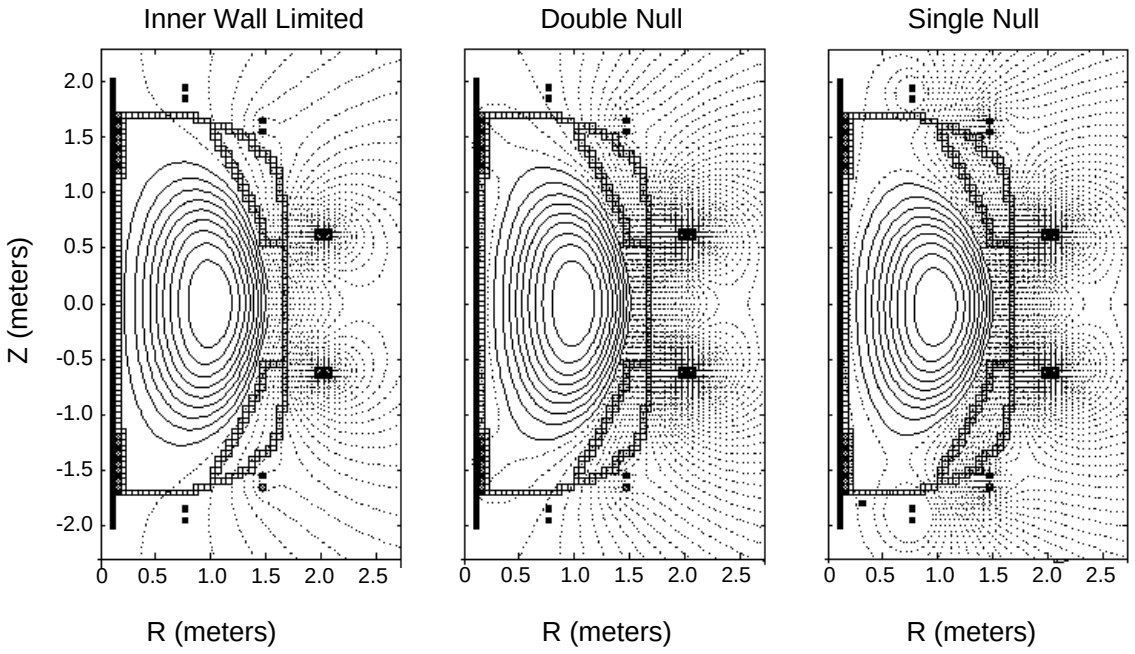

Figure 2: NSTX Configurations

example, Fig. 2 shows three reference configurations; inner wall limited, double-null X-point, and single-null X-point. The single null X-point configuration, as noted in the previous section, is necessary for CHI. For the NSTX configurations, the vertical field is provided mainly by PF3 and PF5, two of the outermost coil sets, while shaping is controlled primarily by the two inner coils, PF1a and PF2. In the inner wall limited configuration, only PF3 is needed in addition to PF5. For the diverted configurations, both PF1a and PF3 are needed in order to move the X-point into the region inside the vacuum vessel. PF1b is needed for fine tuning the position of the X-point and separatrix legs in the single-null configuration for CHI.

The range of accessible elongation and triangularity has been computed and is shown in Fig. 3. In this calculation, both first stability regime ($q_0 \sim 1.0$) and advanced physics regime ($q_0 \sim 2.5$) configurations were considered. From the figure it can be seen that a range of shapes can be produced. This capability allows the exploration of the dependence of MHD stability and confinement on these parameters. The flexibility also allows for the adjustment of shapes for ameliorating high heat fluxes on the divertor plates. The results shown here used only the coil current and power supply limits as constraints, with no consideration given towards MHD stability properties. It is to be noted that while the entire range of shapes can be produced within the power supply and coil current limits, these limits are challenged for PF2 and PF3 for low elongation and low triangularity double-null plasmas. The

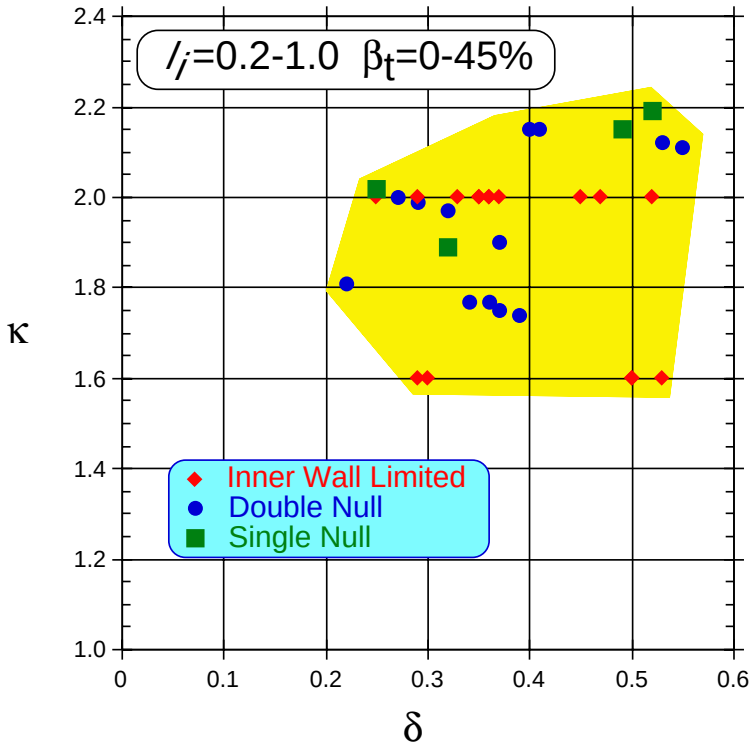

Figure 3: NSTX shape flexibility for inner wall limited (IWL), double and single null configurations.

reason for this is the high natural elongation of ST plasmas. For NSTX, the natural elongation is above 2 at the low l_i values ($\leq$6) expected to be produced. To reduce the elongation to values near 1.6 requires sufficient current in PF2 and PF3 to counteract this natural elongation, and the required currents in these coils can be close to the mentioned limits. This is not the case for the inner wall limited plasmas. It is also possible to produce inner wall limited plasmas with $A = 1.4$ and $\kappa = 3$. However, these plasmas, with $R = 0.7\ m$ and $a = 0.5\ m$, would be too far from the conducting plates to gain the benefit of the enhanced vertical and MHD stability that the plates provide.

NSTX is also capable of producing plasmas with varying aspect ratio, from the nominal value near 1.25 up to 2.0, all within the coil capabilities of the device. This is important for the MHD stability and confinement studies, not only because of the direct connection that can be made with the conventional, higher aspect ratio database, but because of the expectation that microinstabilities are expected to be suppressed with decreasing aspect ratio, and the ability to scan in R/a will facilitate the direct study of this effect.

V. Physics Focus Areas

A. Confinement and Transport

One of the primary mission elements of NSTX is to determine the confinement scaling at low aspect ratio and make a connection between this scaling and those at the higher, more conventional aspect ratio for which a multitude of global confinement scalings have been developed. The only information about confinement behavior at low R/a with auxiliary heating comes from START.[1] START operated with Neutral Beam Injection whose powers ranged up to approximately 0.8 MW. These power levels were comparable to the OH heating power levels. START plasmas exhibited characteristics of H-mode plasmas; increase in line averaged density, flat density profiles with steep edge density gradients, and ELM-like behavior. The deduced confinement times agreed well with one to two times some popular L-mode scalings, most notably the Lackner-Gottardi-Connor scaling (Lackner-Gottardi with a low aspect ratio correction made by Connor).[22,23] This scaling has parametric dependences generally similar to those of ITER89-P,[11] but with a stronger size and density dependence.

The H-mode should be easily attainable in NSTX, based on the predictions of various L- to H-mode scaling expressions. While no one expression has been accepted as the standard for determining the threshold power, several expressions do a reasonably good job in describing the lower threshold boundary for "easy transition" discharges.[24] Using the baseline NSTX parameters, these expressions give a range for the threshold power level from tens to 150 kW, indicating that the H-mode should be accessible in NSTX plasmas, which will be heated at the multi-MW power levels.

As discussed in the Experimental Objectives section, the NSTX performance goals include achieving β_t (β_n) values of $\sim$25% (4) for first stability regime plasmas, and up to 40% (8) in advanced regimes. Estimates of the power required to attain these values are shown in Fig. 4. Plotted in the figure is the achievable β_t (β_n) as a function of heating power for confinement enhancements of 1, 2, and 3 relative to the ITER97L scaling.[13] This is a recently developed L-mode scaling which has parametric dependences similar to those of ITER89P, but which is about 10% more pessimistic (i.e., lower confinement times) than ITER89-P, and about 70% more pessimistic than Lackner-Gottardi-Connor for the NSTX baseline parameters. An enhancement factor of 2.0 applied to ITER97L gives the same confinement time as applying an enhancement factor of about 1.2 to Lackner-Gottardi-Connor (which for NSTX baseline parameters is about 40 msec). What is seen from the figure is that the high-β target is accessible with about 4 to 5 MW of heating power at the highest enhancement factor,

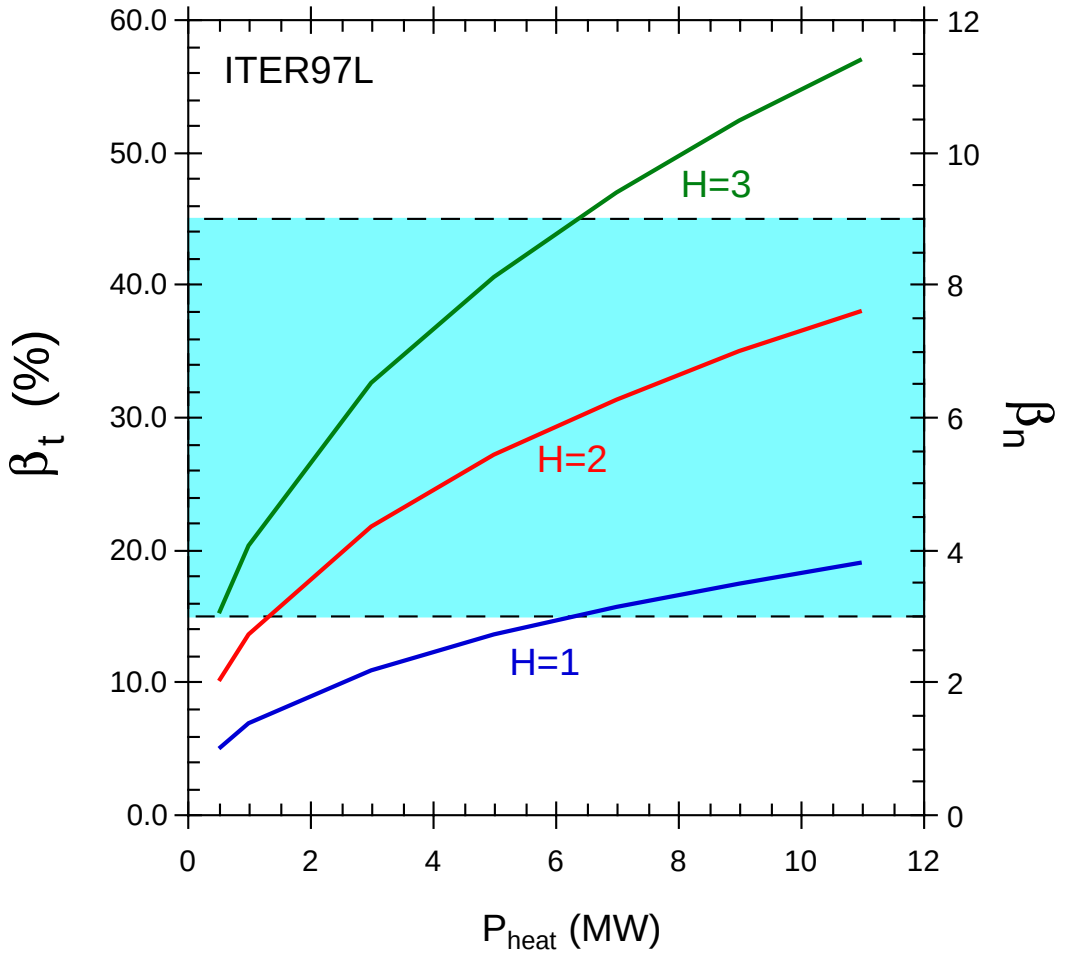

Figure 4: Achievable β_t, β_n as functions of auxiliary heating power for three different enhancement factors relative to ITER97L scaling.

but that approximately 11 MW of power is needed to achieve this target at H=2. The highest β_t values are not accessible for H=1 using this confinement expression. At high β_t, the "volume averaged" electron collisionality ($\propto < n_e > / < T_e >^2$) is comparable to what would be expected in an ST fusion core.

The ability to produce low collisionality plasmas with strong auxiliary heating, as well as the ability to operate over a range of aspect ratio, allows NSTX to explore the benefit of low aspect ratio in suppressing both electrostatic and electromagnetic transport-inducing microinstabilities. The expected behavior of these instabilities was studied using a comprehensive kinetic toroidal microinstability code which takes into account high-n effects, all resonances, finite-β, finite-Larmor radius, and banana orbit effects.[5] The study was performed for plasmas at fixed q_* ($\equiv q_{cyl}(1+\kappa^2)/2$) and RB_T, over a range of aspect ratio from 1.25 to 2.5. The results show that both the kinetic

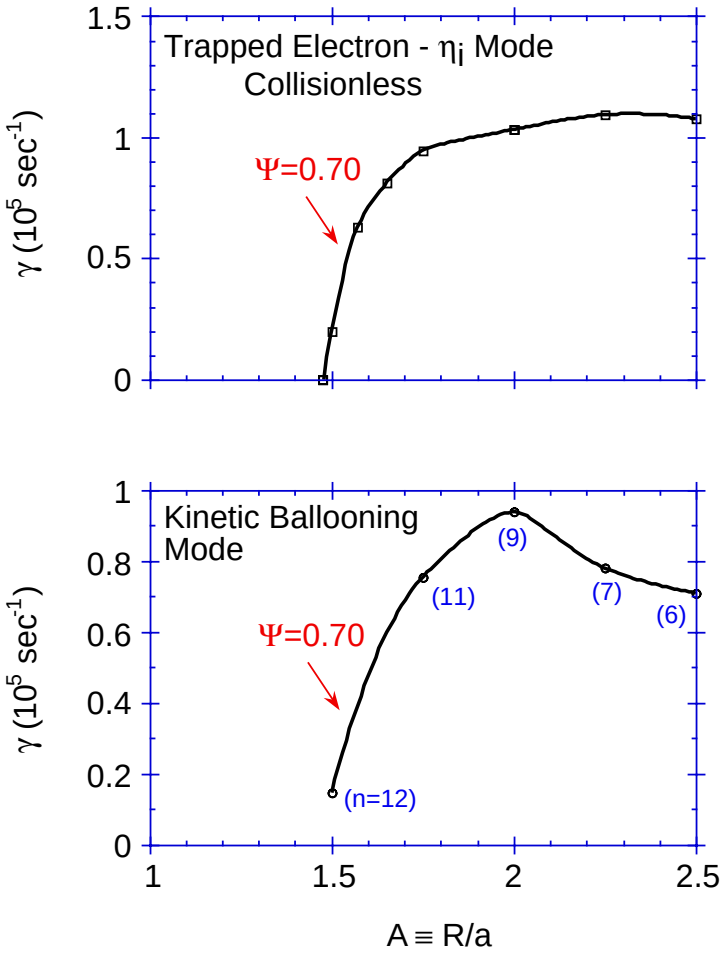

Figure 5: Growth rates as functions of aspect ratio for electromagnetic and electrostatic modes.

ballooning mode (electromagnetic) and the trapped electron-η_i mode (electrostatic) are suppressed as the aspect ratio is lowered. The growth rates are plotted as functions of aspect ratio for both modes at the $\Psi = 0.7$ flux surface in Fig. 5. The "n" numbers for the electromagnetic mode are the toroidal mode numbers of the most unstable mode on that surface. As can be seen, the growth rates start to decrease sharply at $R/a \sim 1.5$, with complete stabilization of these modes on this flux surface at $R/a \simeq 1.3$ to 1.5. The reason for stabilization of these modes with decreasing aspect ratio can be linked to the strong toriodicity of these plasmas, which leads to a reduction in the orbit-averaged bad curvature (the instability drive).

In addition to the effect of reduced orbit-averaged bad curvature, the low toroidal field of NSTX is an advantage with respect to flow shear for stabilization of microturbulence. Because the toroidal field is approximately one order of magnitude lower

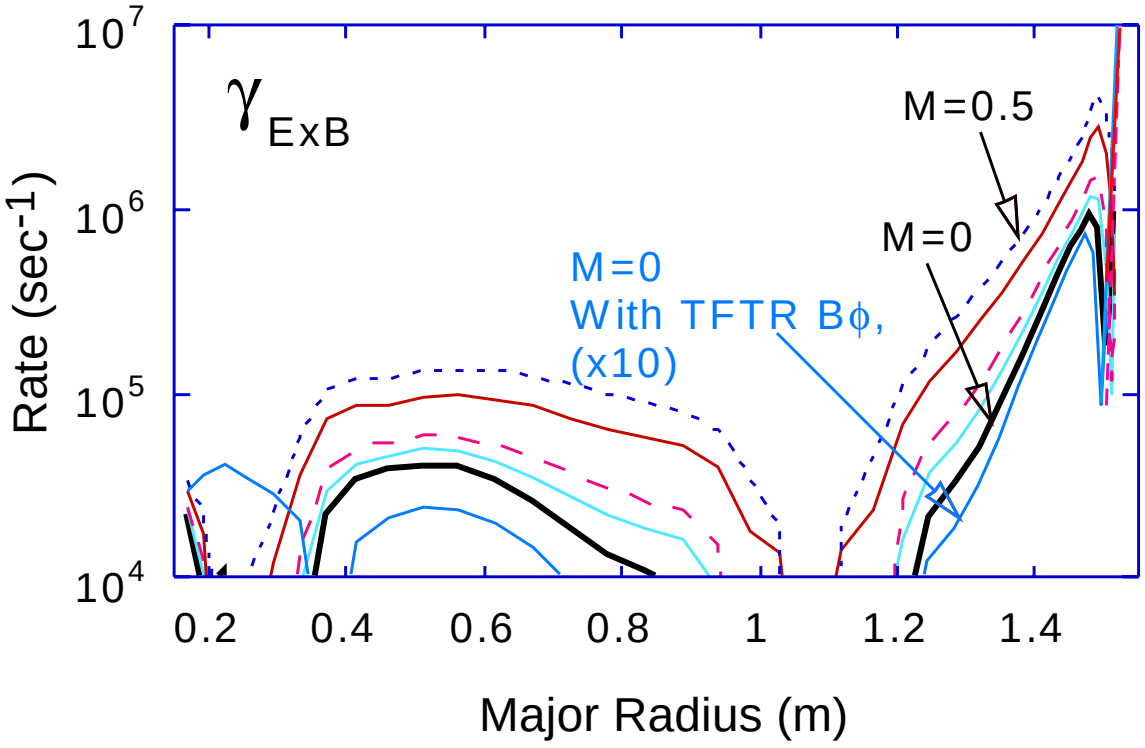

Figure 6: NSTX $E \times B$ shearing rate profile for different Mach numbers. Also shown for comparison is the shearing rate profile for TFTR ($\times 10$).

than that at conventional aspect ratio, the damping due to sheared flow will be strong. The shearing rate due to $E \times B$ flows is given by

$$\gamma_{E\times B} = \frac{RB_\theta}{B}\frac{d}{dR}\left(\frac{E_r}{RB_\theta}\right) \tag{9}$$

where the E_r is composed, primarily, of one term proportional to the plasma pressure gradient and one term proportional to the toroidal flow .[25] Both terms can be important in NSTX. Fig. 6 shows the shearing rate for NSTX assuming broad pressure profiles optimized for MHD stability (see next section), and different toroidal flow Mach numbers. The influence of the toroidal flow can be seen by the difference in shearing rates at different Mach numbers. The shearing rates themselves in the outer portion of the plasma ($R \geq 1.1\ m$) can be up to an order of magnitude higher than the growth rates shown in Fig. 5. Turbulence suppression occurs for $\gamma_{E\times B} \geq \gamma_{mode}$. It is also seen that the shearing rate with a TFTR-magnitude toroidal field is at least an order of magnitude lower than that in NSTX for the same Mach number.

B. Stability and β-Limits

Results on the axisymmetric and MHD stability properties of NSTX will be presented in this section.

The same self-fields that provide the natural elongation in ST plasmas through their vertical component provide a radial component that acts to slow down the ST plasmas vertical motion, thus enhancing its axisymmetric stability properties relative to those at conventional aspect ratio. Calculations were carried out using the TSC and TEQ codes to examine the vertical motion growth times in NSTX. The growth time is simply the inverse of the growth rate of the vertical instability. For these calculations, realistic models of the vacuum vessel, conducting plates and connectors were used. With the conducting plates in place, the growth times for nominal NSTX plasmas with $l_i = 0.6$, $\kappa = 2.0$ and β_t=16% is quite long, between 250 and 300 msec with the plates in place. For comparison, the vertical motion growth time for this plasma without the plates is of order msec, which is still considerably longer than that at conventional aspect ratio. The growth time (with the plates) is not a strong function of β, remaining approximately constant as β_t is raised to 40% and decreasing to about 100 msec as β_t is lowered to a few percent. A larger variation is seen as a function of l_i, however. Fig. 7 shows the vertical growth time as a function of l_i for double-null plasmas with β_t=13%. As can be seen, the maximum growth time occurs near $l_i = 0.5$, and it decreases to 0.12 sec at $l_i = 1.0$ due to an increase in the effective distance between the conducting plates and the current centroid as the current profile becomes more peaked. The vertical growth time also decreases dramatically by an order of magnitude as l_i is lowered toward 0.3. This reduction is due to the non-rigid motion and strong deformability of plasmas at low l_i with discrete passive stabilizers.[26,27]

In order for a compact spherical torus reactor to be attractive, it must operate at high-β_t, with β_t values typically $\geq$30%. Because of this, MHD stability is a key issue at low aspect ratio. This discussion of MHD stability issues in NSTX will just highlight a more detailed discussion that is presented in Ref.[4]

Previous MHD stability studies at higher aspect ratio have identified the importance of certain dimensionless parameters which are useful in predicting MHD stability. The two most widely recognized are $q_* = (2\pi a)^2 B_0(1+\kappa^2)/(2\mu_0 R_0 I_p)$ and the normalized beta, $\beta_n = \beta_t a B_0/I_p$. In general, kink modes limit the amount of plasma current, thus setting a lower limit on q_*. Pressure driven modes, such as high-n ballooning modes, intermediate-n infernal modes, and low-n kink modes, tend to limit the plasma pressure which can be contained with a given external magnetic

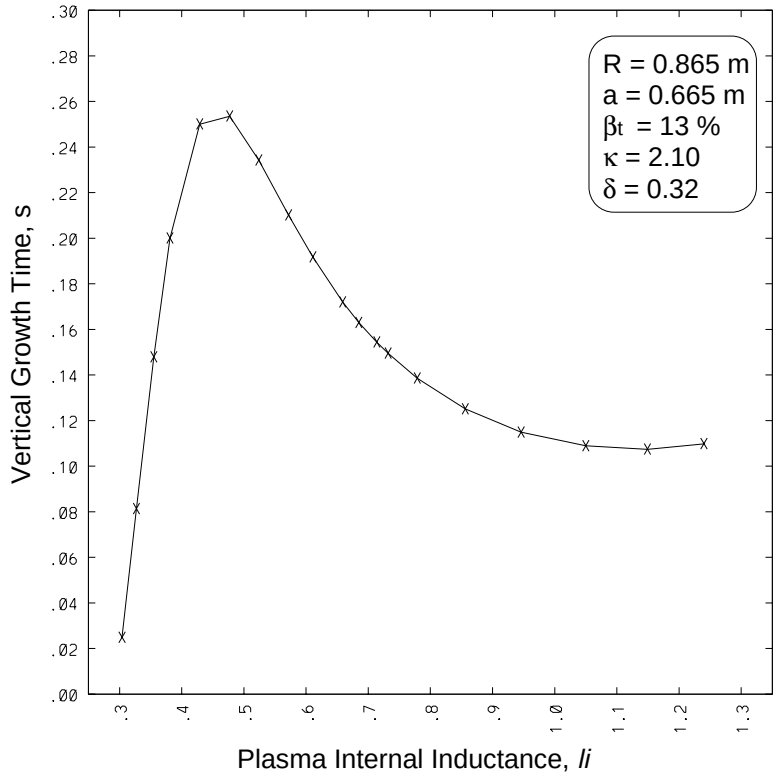

Figure 7: Vertical motion growth times as a function of l_i for an NSTX plasma with β_t=13%

field. At high aspect ratio, the β_n limit is 3 to 4 for first stability regime plasmas and 5 to 6 in the advanced physics (or second stability) regime.

A series of numerical scans were performed to determine the possible range of stable equilibria in NSTX-like plasmas ($R/a = 1.2 - 1.45$, $\kappa = 1.6 - 2.2$).[4] The stability of the equilibria was determined using the PEST-II code for low-n kink stability and the BALLOON code for high-n stability. Three distinct regimes were noted. The first is operation at high-β_t (β_n=5-6) and low q_* ($\leq$ 2). This regime typically is at low $\epsilon\beta_{pol}$ (≈ 0.5), and, therefore, has a low bootstrap fraction ($\approx 40\%$). Equilibria in this regime require substantial current drive, and therefore would not be suitable for a self-sustaining fusion core. A second regime with higher β_t and bootstrap fraction exists, in which $q_0 > 2$, $\epsilon\beta_{pol} \simeq 1.0$, $\beta_n \simeq 8$, and a bootstrap fraction of up to 80%. These cases rely only on edge current drive to suppress edge-localized ballooning modes. The third regime is nearly fully bootstrapped, requiring only core current drive. These plasmas have high $\epsilon\beta_{pol}$ (1.5), but are limited in β_t.

In detailed calculations, the benefit of low aspect ratio is clearly seen. Fig. 8 shows the results of a scan in aspect ratio for a conventional, first stability regime, configuration ($q_0 = 1.1$) with a broad pressure profile ($p_0/ < p >= 1.8$), at κ=1.6, which is an elongation that is slightly less than the baseline design case of 2.0. Marginal stability points are shown for a case with $q_*/q_0 = 1.5$ and $q_0 = 1.1$. For aspect ratios other than 1.2, the conformal wall is at $r_{wall}/a = 1.4$. At $R/a = 1.2$, the wall is at $r_{wall}/a = 1.2$. The results show a marked increase in achievable β_n as aspect ratio decreases, especially for the low-n modes. The effect of the wall is also seen, as the marginally stable β_n increases significantly, especially for the n=1 mode. In these conventional cases, however, it is the $n = \infty$ ballooning mode that sets the upper limit on achievable β_n at low R/a.

The results of a calculation showing the marginal β values for a fully optimized equilibrium is shown in Fig. 9. For this equilibrium, $q_0 = 2.83$, $q_*/q_0 = 0.69$, and the actual locations and extent of the conducting plates were used. Both the β and bootstrap fraction were optimized for this target plasma. It is seen in the figure that for this case the overall β-limit is set by the n=1 mode, to a value of 41.5% (β_n=8.2). Higher-n modes show higher β-limits, with the limit decreasing to $\sim$ 43% ($\beta_n \sim 8.6$) for the infinite-n ballooning mode. There is also a current-driven n=1 mode whose stability depends on the edge q value, with q(a) just above an integer being the most stable (here, q(a)=12.1). The n=2 to 5 kink modes do not appear to show this q dependence, and they have stability limits determined by pressure alone. For this optimized case, the total ∇p-driven current fraction is just over 70%.

The optimized equilibrium and profiles are shown in Fig. 10. The pressure profiles

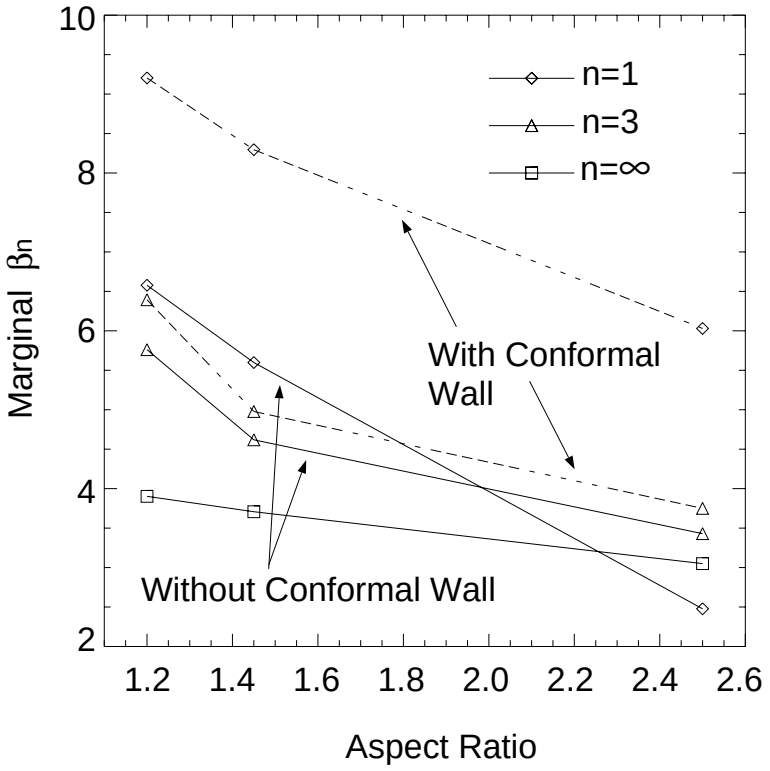

Figure 8: Marginally stable β_n for kink and ballooning modes as a function of aspect ratio for $q_*/q_0 = 1.5,\ q_0 = 1.1$ (first stability regime). Solid lines indicate no conducting wall, dotted lines indicate a conformal wall. The n=∞ (ballooning) mode, which is not influenced by the conducting wall, limits the β_n to ≤ 4 in these unoptimized cases.

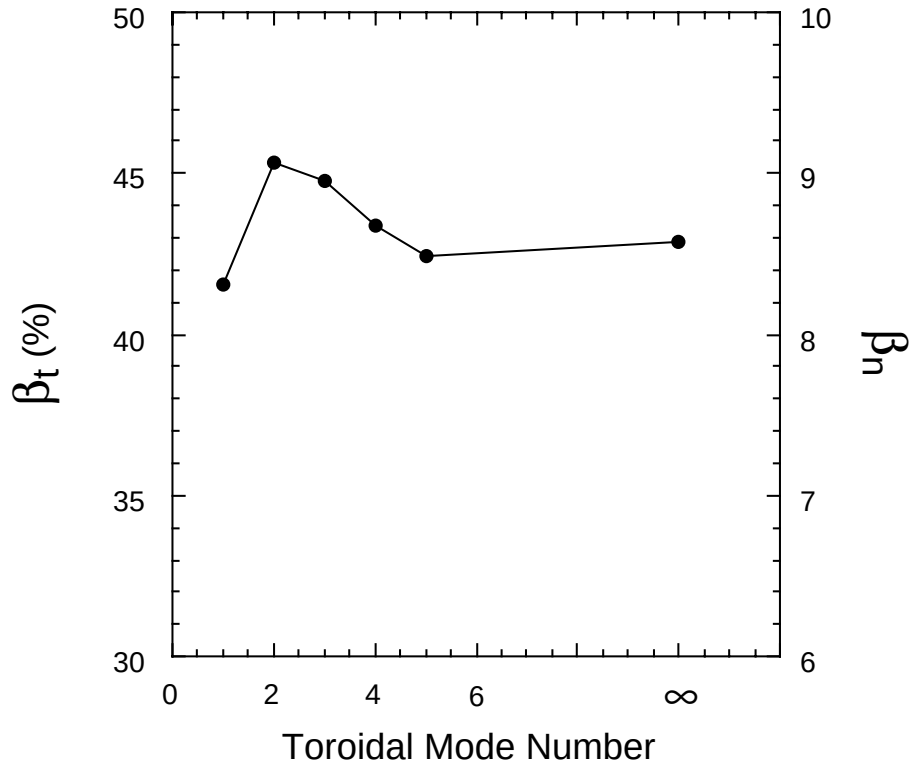

Figure 9: Achievable β_t, β_n as functions of toroidal mode number for optimized pressure and current profiles.

(c) for this optimized equilibrium are relatively broad, and the q-profile (b) remains monotonic despite the hollow total current density profile (d). It can be seen from the panel showing the current profiles that for this equilibrium, the 30% of the current not carried by the bootstrap current, denoted "CD" in the figure, must be driven primarily in the outer region of the plasma. In actual operation, both CHI and HHFW will be used in an attempt to drive current in this location in order to sustain the MA fully non-inductively.

One of the issues for effective passive stabilization is plasma rotation. This area is presently being studied for application to NSTX. One possibility is the natural rotation induced by RF current drive,[28] while another is the electromagnetic torque induced by appropriate phasing of a toroidal array of magnetic coils.[29] A tested method for inducing plasma rotation is through neutral beam injection, a system which is planned to be operational within two years of first plasma.

C. Heating and Current Drive

An ST reactor design precludes an OH solenoid for two essential reasons. The first is that the center stack must be made as thin as possible because the inboard gap has such strong leverage in ST reactor economics, as shown in Sec. II. The second is the neutron damage on insulating materials that would inevitably occur. In addition to these, a compact ST reactor requires a high, steady-state current, typically 20 to 30 MA. These reasons make non-inductive current drive an essential element of an ST reactor. The non-inductive current drive can come from various sources; RF, neutral beams, and bootstrap current are the proven means. The bootstrap current, which can account for up to 75% of the total current in NSTX discharges, was discussed in the previous section. RF current drive can be considered after first noting that the plasma dielectric constant, $\omega_{pe}^2/\omega_{ce}^2 \gg 1$ for low aspect ratio. In fact, for typical NSTX parameters, this value is about 45. At this value, both Lower Hybrid and Electron Cyclotron waves have severe accessibility problems.

High Harmonic Fast Waves (HHFW) are a promising alternative for heating and current drive at low aspect ratio. HHFW show strong single-pass absorption for high-β operation, consistent with the high density, low toroidal field regime of NSTX. HHFW have good accessibility, and will damp primarily on the electrons. At high ion β values, ion absorption can become important. The advantage of HHFW is that the electron heating can enhance bootstrap fractions, and the power deposition can be localized to some extent for profile control. Operation of HHFW on NSTX will nominally be at 30 MHZ (15^{th} harmonic), and it will employ a 12-strap antenna

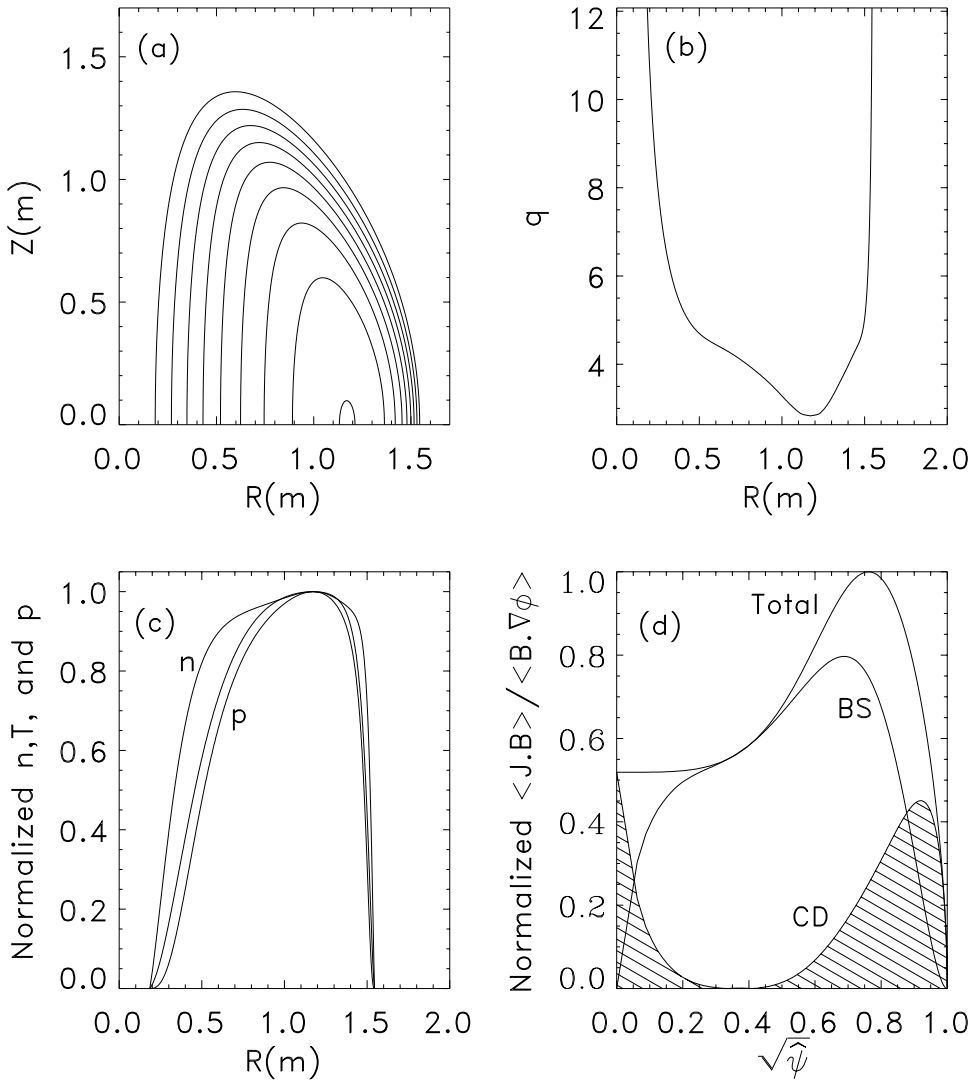

Figure 10: Equilibrium and optimized profiles for the high-β_t target plasma. Shown are the (a) plasma equilibrium, (b) q-profile, (c) normalized density, temperature and pressure profiles, and (d) current profile. The curves labeled BS and CD correspond to the bootstrap current profile and the current driven by external sources respectively. $\hat{\psi}$ is the normalized poloidal flux.

situated at the midplane. Ultimately, 6 MW of RF power will be delivered.

It is necessary to deliver this high power over a range of plasma conditions, for not only will the HHFW be used to heat the plasma and drive current during the high-β sustainment phase of the discharge, but it will be necessary to heat the target OH plasma when β and the temperatures are relatively low. The RANT[30] and PICES[31] codes were used to study the coupling and deposition of HHFW power into various NSTX plasma equilibria. The HHFW current drive profiles were estimated using the Ehst and Karney formulation[32] with trapped electron effects.

The calculation results show that the most promising regime for current profile control appears to be in the β_t=15% range, with the 6 MW of RF driving up to 0.4 MA of current. Fig. 11 shows the results of the calculations for β_t=5% and 25% equilibria for various antenna phasings. In the 5% case ($T_i(0) = T_e(0) = 1\ keV$), penetration to the core is good for all phasings, although there is not full single-pass absorption. Nevertheless, the results indicate that the HHFW will be effective in heating the plasma and driving up to 0.4 MA of current during this phase. For the 25% case, the single-pass absorption is good, with the power being deposited off-axis, as can be seen in the figure. Up to 0.3 MA of current is driven in this scenario for the 30° and 60° phasings. The current drive for the 90° phasing case is poor (0.1 MA) due to the slow phase velocity of the wave, and the deposition profile being farther off-axis, which puts the wave power into the trapped electrons.

Neutral Beam heating and current drive has been estimated for 5 MW of near-tangential injection into nominal NSTX equilibria (β_t=25%). The estimates are based on TRANSP calculations, which use a full-orbit Monte-Carlo package to compute the neutral beam deposition. TRANSP does this calculation in a self-consistent fashion, computing the internal equilibrium as well. The beam that will be used for NSTX is the spare TFTR neutral beam, consisting of three sources of deuterium at 80 keV, with the central source being injected at a tangency radius of 0.7 m, and the two adjoining sources at $\pm$0.1 m. The calculation indicates that only a few hundred kW of heating power will be lost through shine-thru, charge-exchange or bad orbits for co-injection, so that most of the heating power will be available for this scenario. About 70% of the heating power is lost for counter-injection, primarily through bad orbits.

In the co-injection scenario, approximately 50% of the fast ions are on trapped orbits. The remaining passing particles impart enough momentum to electrons to drive approximately 0.2 MA of current. While the 0.2 MA is not enough to sustain the 1 MA current fully non-inductively, it can play an important role in conjunction with other current drive techniques and bootstrap current. Both the heating and

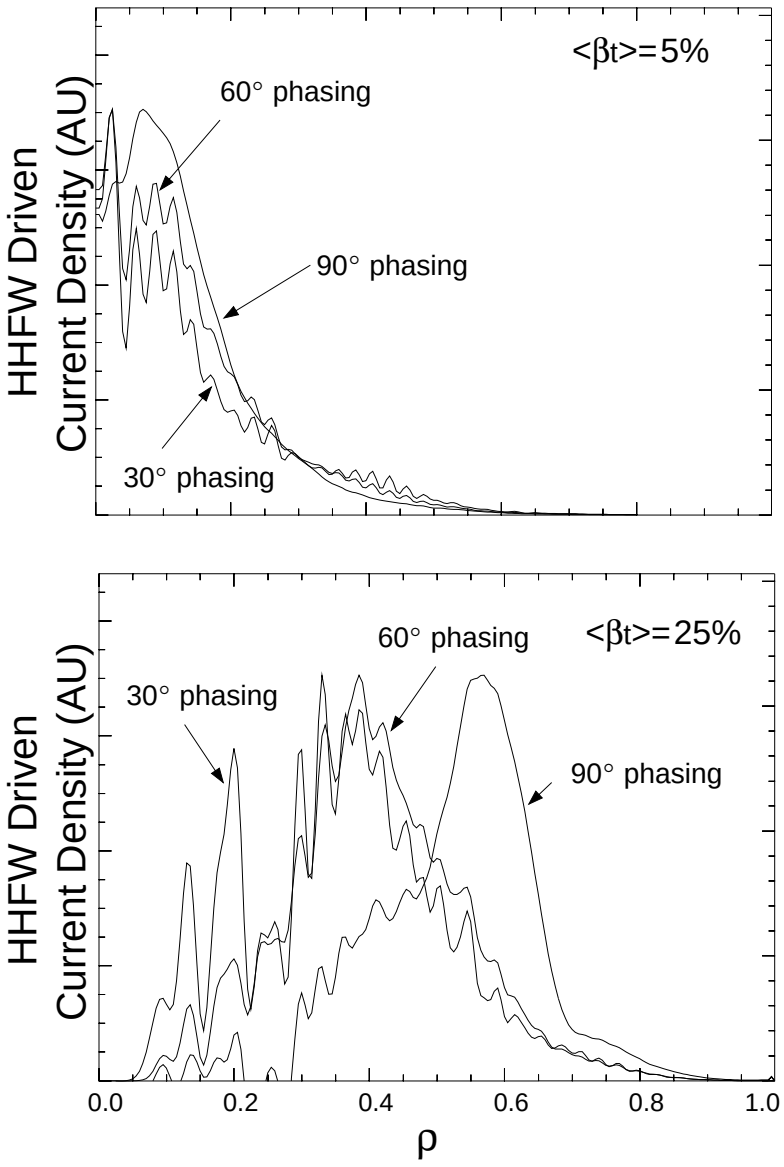

Figure 11: Current density profiles driven by the HHFW for different antenna phasing and plasma β values. ρ is the square root of the normalized toroidal flux.

current drive profiles for NBI are peaked on-axis.

Co-axial Helicity Injection will be used to aid plasma start-up and potentially to help sustain the full 1 MA current by current drive in the outer region. CHI delivers poloidal flux to the plasma edge through the use of biased electrodes, and this flux (toroidal current) is transported throughout the plasma via global MHD fluctuations. Approximately 0.2 MA of plasma current has been driven in HIT with CHI[3] with a 10% conversion efficiency (injector current /driven current) at temperatures of $\approx 100\ eV$. From a physics perspective, NSTX provides an excellent 1 MA testbed for CHI at low aspect ratio. As discussed earlier in this section, it is expected that other non-inductive current drive schemes in NSTX can provide up to 75% of the full current. It would therefore be necessary for CHI to provide approximately 0.25 MA of current during the flattop phase of the discharge for fully non-inductive current sustainment, and approximately 0.5 MA of current during start-up. Given the available hardware and assuming the same 10% conversion efficiency, and given the larger size of NSTX relative to HIT, these levels of driven current should be achievable.[8]

D. Reference Discharge Scenarios and Plasma Performance

Details of simulations of reference discharge scenarios, including possible plasma performance and current flattop duration over a wide range of heating scenarios will be discussed in this section. The Tokamak Simulation Code (TSC) was used for these simulations. TSC is a time-dependent, free-boundary, predictive equilibrium and transport code whose strength lies in its ability to aid in the scenario development of both discharge energetics and plasma control systems. TSC solves the fully dynamic MHD/Maxwell's equations coupled to transport and Ohm's Law equations. TSC requires as input the device hardware and complement of coils and their respective electrical characteristics, assumptions concerning the plasma density profile (or a particle diffusivity), impurities, global discharge characteristics, PF coil currents, and position control feedback requirements. A more complete description of the code can be found in Refs.[33,34] TSC is not used to model plasma breakdown; these calculations, done using other codes, indicated the adequacy of the PF coils and associated power supplies for creating the field nulls necessary for inductive-only plasma initiation. The minimum stray field requirements are expected to be mitigated with the planned use of EC preionization.

TSC simulations were carried out for OH, RF, and NB-heated scenarios. For all these simulations, the multiplier of the plasma energy diffusivity, which is based on the Tang-Coppi model,[35] was adjusted in order to give a global confinement time

comparable to the Lackner-Gottardi-Connor L-mode value, consistent with recent START NB-heating results. A typical reference discharge for an RF-heated inductive scenario is shown in Fig. 12. In this simulation, the current was initiated at time=0 at a value of 20 kA, and then, under a current feedback control scheme, was ramped inductively at a rate of 5 MA/sec to the full 1 MA, and then held at that level. Six MW of HHFW heating was turned on at 0.1 sec, with the heating producing a central electron temperature of about 4 keV at a line averaged density of 3.7×10^{19} m^{-3}. The density profile was assumed to be broad, and given by

$$n(\psi, t) \propto n_0(t) \left[1 - \left(\frac{\psi - \psi_{min}}{\psi_{lim} - \psi_{min}} \right)^6 \right]^{0.5} \tag{10}$$

The RF deposition profile was input into the calculation, and it was taken to be peaked on-axis during the initial phase of RF heating (0.09 to 0.2 sec), and then it was taken to be peaked off-axis thereafter, consistent with the modeling results from the RANT and PICES codes (see earlier section on Heating and Current Drive). For this and other inductive discharge simulations reported here, no RF-current drive was assumed, although the calculated bootstrap current drive, amounting to ≈ 300 kA by the end of the flattop phase, was included. The omission of the RF-current drive leads to a conservative estimate of the possible current flattop duration.

In the bottom of the figure is the OH solenoid current necessary to produce the pre-programmed plasma current as a function of time. The OH current started at approximately +24 $kA/turn$, and then decreased in time to its minimum value of approximately -22 $kA/turn$, at which point a total of $\sim$ 0.9 V-sec of flux has been produced (2/3 of this by the OH). At this time, the 1 MA current has been sustained for about 0.5 sec, giving a total pulse length, including the current ramp-up time, of 0.7 sec. The plasma current is then ramped down over the next 0.4 sec.

The scenario shown in Fig. 12 was just one of the scenarios studied. Also simulated were scenarios with different plasma current ramp rates and different heating scenarios. The change in rate of V-sec consumption from slowing the plasma current ramp-up rate down by even over a factor of two did not change the ultimate flattop duration much. For RF heated discharges, the flattop duration remained in the 0.4 to 0.5 sec range. With NBI instead of RF-heating, the current flattop duration decreased to $\sim$ 0.15 sec, owing to a larger rate of V-sec consumption, both resistive (colder electrons) and inductive. There is virtually no current flattop duration at 1 MA for OH-only heated plasmas; 1 MA can be attained but not sustained. However, current flattop durations up to 0.5 sec can be achieved in OH plasmas at maximum current levels of 0.5 MA, and over 1 sec flattops can be achieved at 0.25 MA. A his-

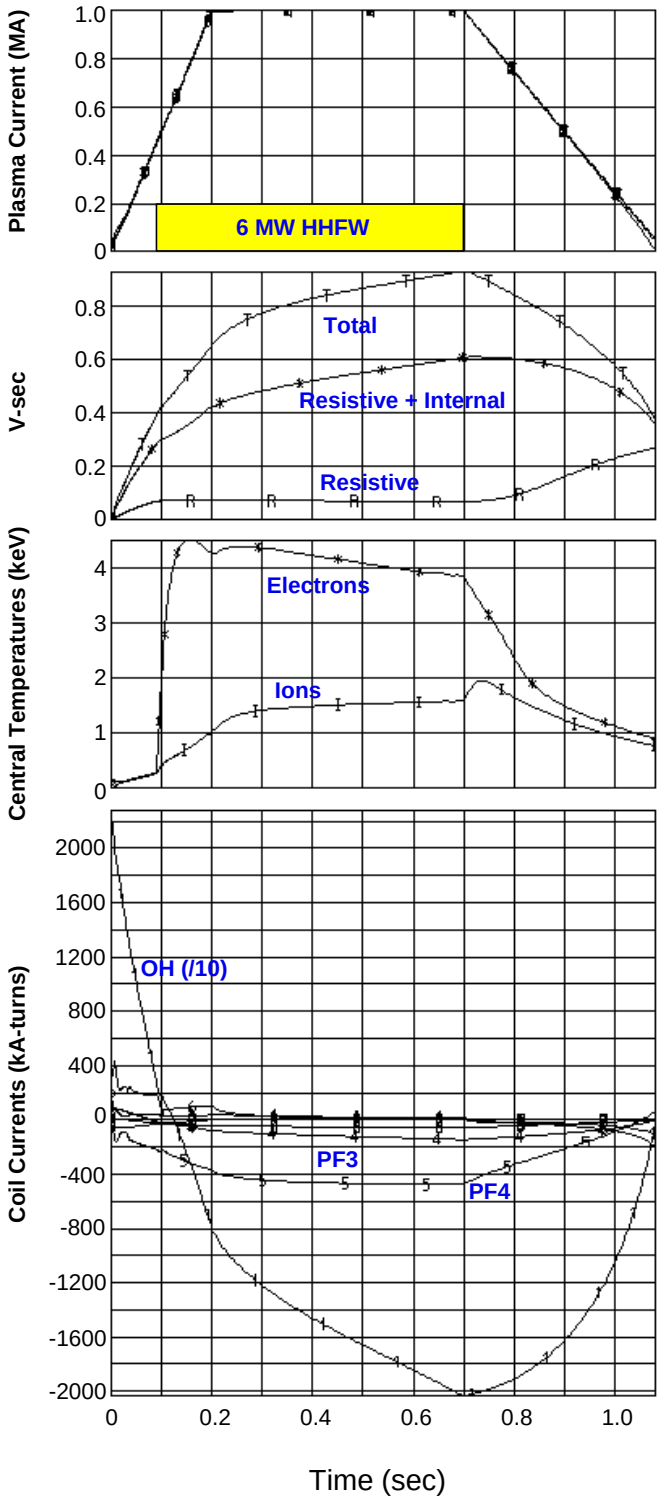

Figure 12: Inductive reference discharge with HHFW heating.

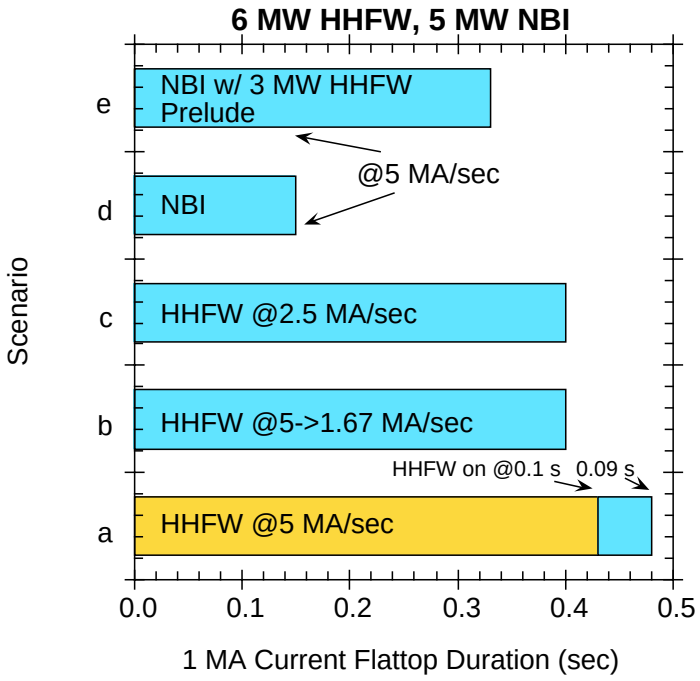

Figure 13: 1 MA current flattop durations for inductive discharges under different heating scenarios.

togram showing the expected current flattop durations for the 1 MA current level is shown in Fig. 13.

The length of the current flattop duration can be enhanced greatly by using the CHI to produce a 0.5 MA target plasma non-inductively, and then using inductive means to ramp the current to the 1 MA level and sustaining it there. This is simply the result of not having to use V-sec to ramp the current to 0.5 MA inductively; therefore, the resulting V-sec savings can be used to extend the current flattop duration. It is seen in Fig. 14 that the V-sec savings results in 1 MA flattops ranging from several hundred msec for OH to over 1 sec with HHFW heating.

NBI heats the ions preferentially while the HHFW heats electrons preferentially. For the transport assumptions and heating profiles used in the simulations, the expected plasma densities and temperatures are given in Table 3, indicating multi-keV temperatures for both species in either auxiliary heating scenario. The neutral beam deposition profile was input into TSC, but was based on the NB deposition profile shape that was calculated in the TRANSP Monte-Carlo code. This profile was peaked on-axis.

In the simulations discussed above, the bulk of the plasma current was driven by inductive means. Fully non-inductive operation with pulse lengths greater than the

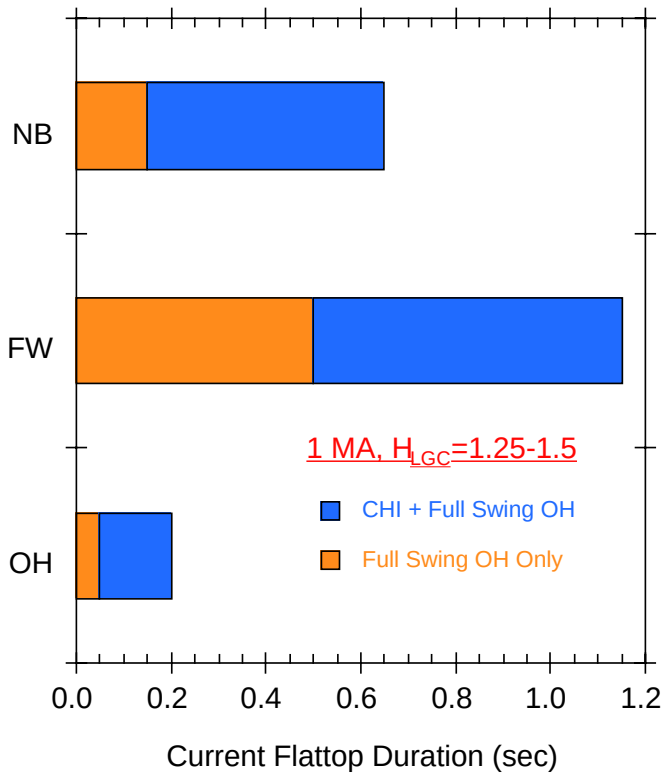

Figure 14: 1 MA current flattop durations for a variety of heating scenarios with and without a 0.5 MA target plasma produced by CHI.

Scenario	$\overline{n}_e\ 10^{19}\ m^{-3}$	$T_e(0)\ keV$	$T_i(0)\ keV$
OH	2.4	0.7	0.7
5 MW NBI	4.7	1.7	2.7
6 MW HHFW	3.7	4.0	1.6

Table 3: Expected plasma performance for different heating scenarios.

current relaxation time is one of the objectives of NSTX. Accordingly, a simulation for a discharge duration of ~ 5 sec was carried out to determine the key elements necessary for producing a non-inductive discharge, and to define the maximum pulse length required for NSTX. For this simulation, twice ITER97L confinement was assumed, and the CHI was assumed to produce a fully elongated, 0.5 MA target plasma with a relatively flat current profile ($q_0 \sim 3,\ q_\psi \sim 10$). Fast wave power of 2 MW was then applied, increasing to 6 MW over the course of 0.6 sec. Accompanying this was a fast wave driven current of 0.4 MA. The current drive profile was initially peaked on-axis, but then the fraction of on-axis current drive was reduced essentially to zero 1.4 sec later, consistent with the PICES calculations of the driven current profile for these plasma conditions. Augmenting this 0.4 MA of HHFW driven current was 0.6 MA of bootstrap current drive, the two mechanisms accounting for most of the full 1 MA of plasma current during this phase. The β_t increased, reaching the 40% level 1.5 sec into the simulation, and remaining constant thereafter.

The toroidal current density profile relaxation is shown in Fig. 15. This figure contains snapshots of current profiles from various time periods during the discharge. The profile starts out relatively flat at 0.2 sec (the start of the simulation), except for the toroidal effects causing the current density on the inside to be greater than that on the outside, consistent with CHI startup. As HHFW current drive and heating is applied, and as the bootstrap current builds up, the current profile becomes hollow, with very low current density in the center due to flux exclusion from trying to drive current there. As the current drive in the central region is reduced, the profile readjusts, but it does not come to a steady-state until two to four seconds into the discharge. This current relaxation time, which is consistent with the simple estimate presented earlier in the paper, defines the pulse length specification of 5 sec. Despite the hollowness of the current profile, the q-profile, which relaxes on the same time scale as that of the current, remains essentially monotonic, with a broad low-shear region across the inner portion of the plasma.

E. Power and Particle Handling

NSTX is designed to produce distinctly different divertor and limiter configurations (Fig. 2): double and single nulls, where the plasma is defined by a separatrix and X-points within the vessel, and a "natural" inner-wall limited configuration, where the outboard SOL is diverted without any X-points at the plasma edge. This capability will permit divertor physics tests of critical importance to future compact ST fusion cores of high power density. The divertor strike plates and plasma facing com-

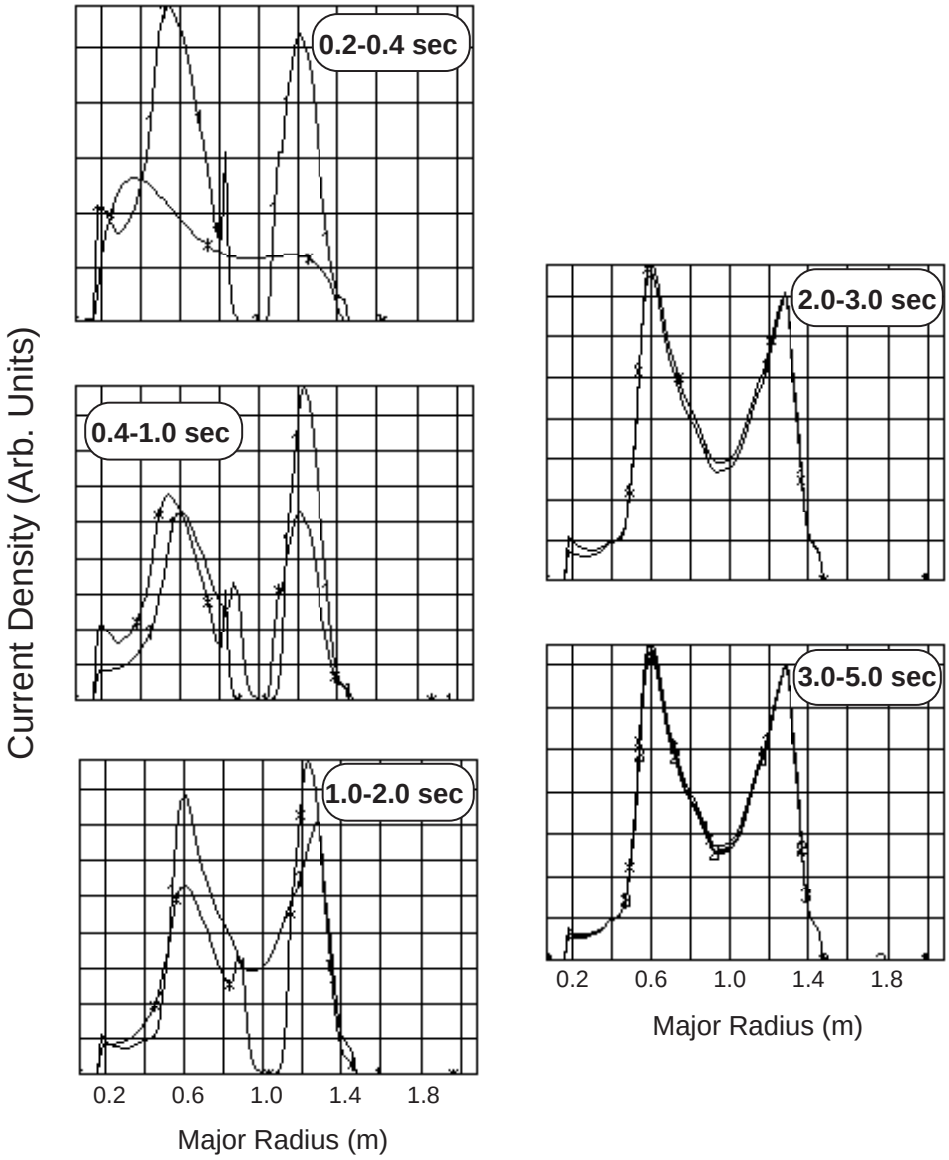

Figure 15: Evolution of current density during non-inductive discharge simulation

ponents must be designed to handle adequately the expected maximum heat fluxes for all configurations for discharge durations of at least several seconds.

In OH-only plasmas, the maximum heating power is expected to be approximately 1.5 MW for a current flattop duration of up to several hundred msec. Such plasmas are not expected to introduce the maximum heat fluxes for NSTX. In auxiliary heated discharges, the baseline design maximum power is 6 MW for a pulse length of 5 sec ($P/R = 7.2\ MW/m,\ P/A_{sep} = 0.2\ MW/m^2$). Neutral beam injection could add another 5 MW of injected power. The peak heat flux to the divertor and center stack tiles has been estimated by simple power balance considerations and corroborated with analytic and 2-D numerical modeling. The peak heat flux in the divertor can be estimated by assuming an exponential heat flux profile in both the divertor and the midplane, and by relating the divertor SOL power flux width to that in the midplane by geometry and flux expansion; i.e., $\lambda_q^{sol} = \lambda_q^{mid} f_{exp}/sin(\alpha)$ where f_{exp} is the poloidal flux expansion from the midplane to the target at the 1 cm flux line and α is the angle of the separatrix and the target in the poloidal plane, measured from the horizontal direction. Power balance requires that

$$P_{target} = q_{peak}^{div}(\lambda_q^{sol} - \lambda_q^{pfr})2\pi R_{osp} \tag{11}$$

where P_{target} is the divertor target power λ_q^{pfr} is the scrape-off layer heat flux width in the private-flux region, λ_q^{div} is that at the target, and R_{osp} is the outer strike point radius. In addition, the divertor target power is related to the heating power, P_{heat}, by

$$P_{target} = P_{heat} f_{out}(1 - f_{rad})/N_{div} \tag{12}$$

where f_{out} is the ratio of power flow in the outer divertor side to the total power flow into the scrape-off layer (SOL), f_{rad} is the radiated power fraction, and N_{div} is the number of divertors (equally) sharing the power. Substituting for λ_q^{sol} and P_{target} in Eq. 11 yields

$$q_{peak}^{div} = P_{heat} f_{out}(1 - f_{rad}) sin(\alpha) N_{div} \lambda_q^{mid} f_{exp}(1 + \frac{\lambda_q^{pfr}}{\lambda_q^{sol}})2\pi R_{osp} \tag{13}$$

Several of the quantities in Eqs. 12 and 13 can be estimated from measurements made on other tokamaks; the remainder are geometry dependent. In the initial NSTX operational phase, a maximum P_{heat} of 6 MW is anticipated; also, N_{div}=2. Based on observations from DIII-D double-null discharges,[36] f_{out}=0.8, f_{rad}=0.3, and $\lambda_q^{pfr}/\lambda_q^{div}$=0.33 are used. Finally, λ_q^{mid} is estimated as 1 cm, as observed in DIII-D

Equilibrium	R_{osp} (m)	f_{exp}	α $(^\circ)$	q_{peak} (MW/m^2)
$l_i = 0.2$ DND	0.79	2.5	60	7.2
$l_i = 0.6$ DND	0.79	5	45	4.4
$l_i = 0.2$ IWL	0.60	5	45	3.8
$l_i = 0.6$ IWL	0.60	10	45	2.1

Table 4: Summary of 0-D heat flux calculations

and other tokamaks.[37] The geometric quantities R_{osp}, f_{exp} and α are equilibrium dependent. Four equilibria are considered: l_i=0.2 and 0.6, DND and inner-wall limited (IWL). For the IWL limited configurations, the P_{target} is reduced by an additional 20% to account for power deposition on the center stack. As shown in Table 4 below, the highest heat flux is observed in the l_i=0.2 DND, due primarily to the low flux expansion.

The largest potential uncertainty in this peak heat flux estimate is the assumed λ_q^{mid}. To corroborate this assumption, the Borass two-point model[38] of the scrape-off layer and divertor was applied to NSTX.[39] This model uses Bohm diffusion for the radial particle and energy transport rates; $\lambda_q^{mid} \sim 1.2\ cm$ is predicted for the NSTX parameters listed above. Finally, 2-D numerical calculations with the b2.5 edge plasma transport code[40] using Bohm radial transport rates predicted a similar λ_q^{mid} and peak heat flux for NSTX.[41]

The peak heat flux to the center stack, $q_{peak,cs}$ is given by

$$q_{peak,cs} = P_{heat}(1 - f_{rad}) f_{iwl} f_{peak} / 4\pi R_{cs} h \tag{14}$$

where f_{iwl} is the fraction of power flow to the inner wall, f_{peak} is a profile peaking factor, R_{cs} is the center stack radius, and h is the center stack height. Note that f_{peak} is needed in this case because Eq. 14 yields the average heat flux for the center stack. DIII-D experiments in marginally inner-wall limited configurations have measured up to 1/2 of the non-radiated power fraction incident on the inner wall ($f_{iwl} \leq 0.5$).[42] As a conservative design, we assume $f_{iwl} = 0.6$ and also that $f_{peak} = 2$. In addition, $R_{cs} = 0.185\ m$ and $h = 1.2\ m$. As in the divertor calculations, $P_{heat} = 6\ MW$ and $f_{rad} = 0.3$. This yields a $q_{peak,cs} \simeq 2\ MW/m^2$.

The thermal constraint on the divertor and center stack graphite tiles is 1200° C, which leaves a 200° C safety margin before radiation enhanced sublimation would result in carbon blooms. 1-D and 2-D time-dependent calculations with the tile engineering design were done to determine the tile thermal response to a heat flux for the full discharge duration of 5 sec., followed by a cool down time between discharges

of 300 sec. The thermal response calculations indicated that the highest computed peak heat flux of 7.2 MW/m^2, which occurs in the divertor, would result in a tile temperature marginally above the constraint (T_{max} = 1200° C). However, this peak temperature would be easily reduced by strike point sweeping, which is within the design capability of the PF coil set, or by nominal gas injection during discharges. The active divertor cooling between pulses will prevent ratcheting of the tile temperature over the course of the day.

2-D calculations of the center stack tiles exposed to a peak heat flux of 2 MW/m^2 indicate a peak tile temperature of $\leq$ 1000° C after several discharges (the center stack tiles are not actively cooled, and thus they are expected to ratchet up during the course of a day). Consequently, the center stack tiles have more safety margin than the divertor tiles with regard to thermal response, but both are expected to be acceptable for the baseline inner-wall limited or double null divertor discharge configurations. Additional heating power or single-null operation will require aggressive heat flux reduction techniques and/or reduction in discharge pulse length.

VI. Diagnostics

The purpose of plasma diagnostics is to provide information on discharge parameters to characterize NSTX plasmas and to guide NSTX operations for optimized performance. The near-term emphasis will be on diagnostics in support of initial NSTX operation, but very shortly thereafter the focus will shift to understanding the basic confinement and transport properties of ohmically-heated NSTX discharges. A list of the Baseline diagnostics and their purpose is given in Table 5.

The long-term objective is to upgrade and expand the diagnostic set for the study of fluctuations, transport and MHD, both in the core and at the edge, in high performance NSTX plasmas. Because of the need for profile measurements to study the transport processes in NSTX plasmas, high priority will be placed on having a multi-pulse Thomson scattering diagnostic available shortly after initial operation. In addition, special emphasis will be placed on developing and installing current profile measurements because of their particular importance. Although there are special challenges for a Motional Stark Effect diagnostic at the low B_T of NSTX, the plan is to have some variant of this technique at time the Neutral Beam system is brought on line. A list of some of the potential Upgrade diagnostics is given in Table 6. New concepts and additional systems developed by the national NSTX team to achieve the Project goals also will be encouraged.

Diagnostic	Measurement
Plasma Current Rogowski Coils	Total plasma current
Eddy Current Rogowski Coils	Halo current monitoring
Flux Loops	Poloidal flux for plasma control
B_θ, B_ρ coils	Magnetic field for control and fluctuations
Mirnov Coils	Magnetic fluctuations
Visible TV Camera	Plasma position and shape for control
IR Camera	Heat loads
Diamagnetic Loop (TF Coil)	Stored energy
Multichannel Bolometer	Radiated power profile
170 GHz μwave Interferometer	Line-integrated plasma density
Survey Spectrometer (SPRED)	Impurities
Visible Spectrometer	Edge/divertor spectroscopy
Visible Bremsstrahlung	Z_{eff} profile
Soft X-ray Imaging	Internal fluctuations, plasma equilibrium
D_α Detectors	Edge recycling
CHERS	Ion temperature profile and toroidal rotation
X-ray Pulse Height Analyzer	Core electron temperature
Neutral Particle Analyzer	Core ion temperature and fast ions
Ultra-Soft X-Ray Array	Start-up and impurity studies
Langmuir Probes/Thermocouples	Divertor parameters

Table 5: Baseline Diagnostics

Diagnostic	Measurement
Multi-pulse Thomson Scattering	Electron temperature and density profiles
Motional Stark Effect	Current profile
Tangential X-ray Imaging	Internal fluctuations
Fission Chambers	Fusion products
Fast Neutron Detectors	MHD activity
Fast Ion Loss Probes	Fast ion loss distribution
FIR Scattering	Fluctuations
Laser-enhanced BES	Fluctuations
Atomic Beam Emission	Edge fluctuations
Fast Edge Imaging	Edge fluctuations
Poloidal CHERS	Poloidal rotation
Fast Reciprocating Edge Probe	Edge temperature and density
Tangential interferometer/polarimeter	Density and toroidal field profiles
Edge Interferometer	Density profile
Heavy Ion Beam Probe	Plasma potential and current distributions
Divertor Bolometers	Radiated power in divertor
Divertor SPRED	Divertor impurities
Divertor Thomson Scattering	Divertor temperature and density profiles

Table 6: Upgrade Diagnostics

VII. Research Plan

The proposed NSTX research plan during the first several years of operation naturally divides into three distinct phases. The first phase of operation, to be conducted after the April 1999 first plasma and a component shakedown period, is the study of start-up and ohmic/low power plasmas The goals of this phase are

- To explore and establish operational space
- To characterize OH/low power confinement and operational limits
- To test and develop HHFW heating scenarios
- To test and develop CHI current initiation

The approach to achieving these goals include inductive operation with EC preionization, vessel and tile conditioning, baseline diagnostics and the multi-pulse Thomson scattering system, and a rudimentary plasma position control system. It is anticipated that, during this period, HHFW powers of up to 4 MW will be injected into the plasma, and currents up to 1 MA with current flattop durations of up to 0.5 sec will be attained. It is expected that this phase will last approximately one year.

Phase II will focus on the heating and non-inductive operations for startup and moderate β_t. The goals of this phase are

- To establish CHI non-inductive startup techniques
- To establish confinement scalings of ST plasmas heated to moderate β_t
- To study local transport and turbulence properties, including transport barrier formation
- To study the approach to β_t-limits at moderate β_t
- To investigate SOL properties for diverted and inner-wall limited configurations
- To explore and characterize current drive during the current sustainment phase (HHFW, CHI and bootstrap)

During this phase, the full 6 MW of HHFW will be injected into the plasma, and the 5 MW neutral beam will be brought on line, the latter enabling the use of NBI-based diagnostics such as MSE and CHERS. Along with these diagnostics, other profile and turbulence diagnostics, as well as SOL and plasma-surface interaction

diagnostics, will be employed. As mentioned, both OH and non-inductive current drive techniques will be used, as will density control techniques in order to achieve high-confinement, high-β_t operation. Aspect ratio scans will be performed to connect the results to those at conventional aspect ratio. The plasmas produced during this phase are expected to have current flattop durations of up to 1 sec, and they are expected to be in the first stability regime ($q_0 \simeq 1,\ \beta_t \leq 25\%$). This phase, in the success oriented schedule, should last for approximately 1 1/2 years.

The third and final phase of operation for the initial NSTX configuration is the advanced physics regime, in which the various tools will be employed to produce and maintain the high performance plasmas. The goals for this phase are

- To achieve fully non-inductive startup and current sustainment at high power for several seconds
- To achieve control of the edge and core transport barriers for good confinement
- To achieve and maintain high-β_t
- To investigate the unique features in an ST plasma edge and SOL

Current profile control will be achieved through the various heating and current drive systems (including a well-aligned bootstrap current), active transport barrier control through pressure profile control, and advanced core and edge diagnostics will be employed. During this phase, in which the plasmas may be in the second stability regime, β_t values of up to 40% and self-driven (i.e., bootstrap) current fractions of up to 75% for pulse lengths of up to 5 sec, are the targets. The duration of this phase may last for several years.

VIII. Physics Summary

The physics investigations discussed above indicate the promise of NSTX in fulfilling its mission objectives to study the basic plasma and fusion related science of low aspect ratio configurations, and to demonstrate the viability of STs in reactor relevant regimes. In particular, NSTX addresses directly the key areas of shaping and configurational flexibility, confinement and transport, MHD stability, non-inductive current drive, and power handling. Operational scenarios, both inductive and non-inductive, are being developed which give guidance on the effects of the various heating and current drive systems, and how various combinations of these techniques will be required for NSTX to achieve its goals.

Specific science issues to be addressed include global confinement properties of ST plasmas at low collisionality, and the suppression of electrostatic and electromagnetic turbulence. Such suppression is expected as the aspect ratio is reduced due to an increase in orbit-averaged good curvature and the low shear on the inboard side of the plasma as the aspect ratio decreases. This suppression is expected to be aided by the high rotational shearing rate due, primarily, to the low toroidal field at low aspect ratio. Furthermore, high-β_t ST configurations, such as the ones to be produced in NSTX, carve out a magnetic well near the magnetic axis, reducing the proportion of trapped particles there and, thus, reducing the instability drive for kinetically driven modes.

NSTX will study the ballooning and kink stability at low aspect ratio and their dependence on variations in aspect ratio, shaping and the presence of the conducting plates, with an aim of producing high-β_t (25-40%) configurations. The role of resistive wall modes and Alfvén eigenmodes at low aspect ratio will be addressed. Operation at high-q, high-β_t, and low collisionality is a prerequisite for high-bootstrap, and thus fully non-inductive operation. NSTX will also determine the lower q-limit for stable, disruption-free operation.

Since plasma pressure and current profile control are important for producing the high-β_t, high-bootstrap configuration, NSTX will employ various means to achieve this goal. Specifically, HHFW will be used to heat the plasma and to drive the current and control the current profile (in the core region at low-β_t, and farther out at high-β_t). HHFW is well suited to ST operation because of its strong single pass absorption and predominant electron heating. CHI will be tested for discharge start-up and for current drive in the outer portion of the plasma during the current sustainment phase.

Important issues in the area of power and particle handling are SOL characterization and the physics that drives transport there. Furthermore, because of its built in shape and configurational flexibility, NSTX will investigate the effect of varying configurations and control schemes in order to reduce divertor heat loads.

ACKNOWLEDGEMENTS

This work was supported by US Department of Energy Contract DE-AC02-CHO3073 at the Princeton Plasma Physics Laboratory, DE-FG02-89ER53297 at Columbia University, DE-AC05-96OR22464 at Oak Ridge National Laboratory, and DE-FG06-90ER54095 at the University of Washington.

References

[1]D. Gates and et al., Phys. Plasmas **5**, 1775 (1998).

[2]M. Ono and et al., Investigation of the effect of resistive MHD modes on spherical torus performance in CDX-U, in *Fusion Energy 1996*, volume 2, page 71, Vienna, Austria, 1997, IAEA, (Proc. 16th Int. Conf. Montreal, 1996).

[3]T. Jarboe and et al., Recent results of the Helicity Injected Tokamak experiment, in *Fusion Energy 1996*, volume 2, page 243, Vienna, Austria, 1997, IAEA, (Proc. 16th Int. Conf. Montreal, 1996).

[4]J. Menard and et al., Nucl. Fusion **37**, 595 (1997).

[5]G. Rewoldt and et al., Phys. Plasmas **3**, 1 (1996).

[6]R. Stambaugh and et al., The Spherical Torus approach to magnetic fusion development, in *Fusion Energy 1996*, volume 2, page 395, Vienna, Austria, 1997, IAEA, (Proc. 16th Int. Conf. Montreal, 1996).

[7]R. Buttery and et al., Steady state spherical tokamaks and future applications, in *Plasma Phys. Cont. Nuclear Fusion Research*, volume 2, page 633, Vienna, Austria, 1995, IAEA, (Proc. 15th Int. Conf. Seville, 1994).

[8]M. Peng and et al., Physics progress towards compact tokamak reactors with normal conducting toroidal field coils, in *Plasma Phys. Cont. Nuclear Fusion Research*, volume 2, page 643, Vienna, Austria, 1995, IAEA, (Proc. 15th Int. Conf. Seville, 1994).

[9]M. Peng and D. Strickler, Nucl. Fusion **26**, 769 (1986).

[10]M. O'Brien and et al., Stability and additional heating properties of spherical tokamak plasmas on START, in *Fusion Energy 1996*, volume 2, page 57, Vienna, Austria, 1997, IAEA, (Proc. 16th Int. Conf. Montreal, 1996).

[11]P. Yushmanov and et al., Nucl. Fusion **30**, 1999 (1990).

[12]D.P. Schissel and the ITER H-mode Confinement Working Group, Analysis of the ITER H-mode confinement database, in *Controlled Fusion and Plasma Physics*, volume 17C, page 103, European Physical Society, (Proc. 20th Eur. Conf. Lisbon, 1993), 1993, Part I.

[13]S.M. Kaye and the ITER Confinement Database Working Group, Nucl. Fusion **37**, 1303 (1997).

[14]M. Roberto and R. Galvao, Nucl. Fusion **32**, 1666 (1982).

[15]R. Galvao, S. Kalmykov, M. Roberto, and W. DeSa, Comments Plasma Phys. Controlled Fusion **15**, 219 (1993).

[16]R. Akers and et al., Ion physics in the START spherical tokamak, in *Controlled Fusion and Plasma Physics*, European Physical Society, (Proc. 25th Eur. Conf. Prague, 1998), to be published.

[17]S. Kaye and et al., Nucl. Fusion **28**, 1963 (1988).

[18]M. Okabayashi and et al., Nucl. Fusion **36**, 1167 (1996).

[19]E. Lazarus and et al., The role of shaping in achieving high performance in DIII-D, in *Plasma Phys. Cont. Nuclear Fusion Research*, volume 1, page 609, Vienna, Austria, 1995, IAEA, (Proc. 16th Int. Conf. Seville, 1994).

[20]M. Ono, Phys. Plasmas **2**, 4075 (1995).

[21]D. Mikkelsen, Phys. Fluids B **1**, 333 (1989).

[22]K. Lackner and N. Gottardi, Nucl. Fusion **30**, 767 (1990).

[23]A. Sykes and et al., Tight aspect ratio tokamak experiments and prospects for the future, in *Int. Conf. on Plasma Physics ICPP1994*, page 110, Woodbury, N.Y., 1995, AIP, AIP Conf. Proceedings No. 345.

[24]F. Ryter and the ITER H-mode Database Working Group, Plasma Physics Control. Fusion **38**, 1279 (1996).

[25]T. Hahm and K. Burrell, Phys. Plasmas **2**, 1648 (1995).

[26]D. Ward, A. Bondeson, and F. Hofmann, Nucl. Fusion **33**, 821 (1993).

[27]C. Kessel, S. Jardin, and G. Neilson, Plasma vertical stability and feedback control for TPX, (15th Int. Symp. Fusion Engineering, Hyannis, Mass, 1993), 1994, IEEE 93CH3348-0.

[28]J. Rice and et al., Nucl. Fusion **38**, 75 (1998).

[29]G. Navartil and et al., Phys. Plasmas **5**, 1855 (1998).

[30]M. Carter and et al., Nucl. Fusion **36**, 209 (1996).

[31]F. Jaeger and et al., Nucl. Fusion **33**, 179 (1993).

[32]D. Ehst and C. Karney, Nucl. Fusion **32**, 1933 (1991).

[33]S. Jardin and et al., J. Comp. Phys. **66**, 481 (1986).

[34]S. Jardin and et al., Nucl. Fusion **33**, 371 (1993).

[35]W. Tang and et al., Nucl. Fusion **26**, 1605 (1986).

[36]T. Petrie and et al., The role of neutrals in the H-L back transition of high density single-null and double-null gas fueled discharges in DIII-D, J. Nucl. Mater., 1998, in press.

[37]C. Lasnier and et al., Survey of target plate heat flux in diverted DIII-D tokamak discharges, Nuc. Fusion, 1998, in press.

[38]K. Borass, Nucl. Fusion **31**, 1035 (1991).

[39]R. Maingi, Edge plasma modeling in STs, Proceedings of Int. Workshop on STs, Abingdon, U.K., 1996.

[40]B. Braams, Contributions to Plasma Physics **36**, 276 (1996).

[41]R. Maingi, 2-Dedge plasma transport calculations for NSTX, Proceedings of Int. Workshop on STs, St. Petersburg, Russia, 1997.

[42]G. Jackson and et al., Plasma Physics **3**, 1005 (1996).